Journal of Power Sources 196 (2011) 7161–7168

Contents lists available at ScienceDirect

Journal of Power Sources

journal homepage: www.elsevier.com/locate/jpowsour

Electrochemical performance of solid oxide electrolysis cell electrodes under high-temperature coelectrolysis of steam and carbon dioxide

Pattaraporn Kim-Lohsoontorn[a], Joongmyeon Bae[b,*]

[a] Department of Chemical Engineering, Mahidol University, Nakorn Pathom 73170, Thailand
[b] KI for Eco-Energy, Korea Advanced Institute of Science and Technology (KAIST), Daejeon 305-701, Republic of Korea

ARTICLE INFO

Article history:
Received 6 July 2010
Received in revised form 6 September 2010
Accepted 8 September 2010
Available online 16 September 2010

Keywords:
Solid oxide electrolysis cell
Solid oxide fuel cell
Steam electrolysis
Carbon dioxide electrolysis
Electrode

ABSTRACT

The SOEC electrodes during steam (H_2O) electrolysis, carbon dioxide (CO_2) electrolysis, and the coelectrolysis of H_2O/CO_2 are investigated. The electrochemical performance of nickel–yttria stabilised zirconia (Ni–YSZ), Ni–$Gd_{0.1}Ce_{0.9}O_{1.95}$ (Ni–GDC), and Ni/Ruthenium–GDC (Ni/Ru–GDC) hydrogen electrodes and $La_{0.8}Sr_{0.2}MnO_{3-\delta}$–YSZ (LSM–YSZ), $La_{0.6}Sr_{0.4}Co_{0.8}Fe_{0.2}O_{3-\delta}$ (LSCF), and $La_{0.8}Sr_{0.2}FeO_{3-\delta}$ (LSF) oxygen electrodes are studied to assess the losses of each electrode relative to a reference electrode. The study is performed over a range of operating conditions, including varying the ratio of H_2O/H_2 and CO_2/CO (50/50 to 90/10), the operating temperature (550–800 °C), and the applied voltage. The activity of Ni–YSZ electrodes during H_2O electrolysis is significantly lower than that for H_2 oxidation. Comparable activity for operating between the SOEC and solid oxide fuel cell (SOFC) modes is observed for the Ni–GDC and Ni/Ru–GDC. The overpotential of H_2 electrodes during CO_2 reduction increases as the CO_2/CO ratio is increased from 50/50 to 90/10 and further increases when the electrode is exposed to a 100% CO_2 (800 °C), corresponding to the increase in the area specific resistance. The electrodes exhibit comparable performance during H_2O electrolysis and coelectrolysis, while the electrode performance is lower in the CO_2-electrolysis mode. The activity of all the O_2 electrodes as an SOFC cathode is higher than that as SOEC anodes. Among these O_2 electrodes, LSM–YSZ exhibits the nearest to symmetrical behaviour.

1. Introduction

In recent years, there has been increasing interest in hydrogen (H_2) as an alternative energy carrier [1]. Because H_2 does not exist readily on Earth as a fuel, it must be generated. Most of the H_2 is currently produced from hydrocarbon fuels [2–5]; however, it results in the liberation of CO_2 and consumes valuable hydrocarbon fuel resources. An alternative method to produce H_2 is via the electrolysis of water:

Steam electrolysis:

$$H_2O \rightarrow H_2 + 0.5O_2, \quad \Delta G = 188.7\,\mathrm{kJ\,mol^{-1}} \tag{1}$$

If the electricity required for this process is derived from renewable energy sources, then this represents a low (or zero) carbon route to H_2 production. Water electrolysis also has the important advantage of producing very pure H_2 without the need for further processing to remove impurities that would negatively impact fuel cell performance durability. Low temperature water electrolysis using a range of alkaline and proton exchange membrane electrolytes has been extensively studied [6–9] and is a commercially available technology. However, the process suffers from low efficiency because of the electrical energy required to meet the enthalpy demand of the reaction. Solid oxide electrolysis cells (SOECs) are under development and have gained much interest. High operating temperatures can reduce the electrical energy requirement of the electrolysis process and, thereby, the cost of H_2 production [10]. Higher operating temperatures improve the electrode kinetics and reduce the SOEC electrolyte resistance, leading to lower losses in cell performance [11–13]. If waste heat from power stations or other industrial processes can be used to sustain the electrolyser operation, SOECs have the potential to generate H_2 at a significantly higher efficiency compared to the low temperature electrolysers [14–16].

The challenge facing the implementation of SOECs remains. High and stable performance is required to reduce the cost of H_2 production. Research is currently aimed at the selection of materials for SOEC components, optimisation of operating conditions, and the effective utilisation of external heat sources. The Sr-doped $LaMnO_3$–yttria-stabilised zirconia (LSM–YSZ) composite is widely used as the cathode in solid oxide fuel cells (SOFCs) and displays good thermal and chemical stability. Nickel–YSZ (Ni–YSZ) is also commonly used as the anode in SOFCs. Because of the similarity to SOFCs, advances have been made in the development of high temperature SOECs based on cell assemblies composed of

* Corresponding author. Tel.: +82 42 350 3045; fax: +82 42 350 3210.
E-mail address: jmbae@kaist.ac.kr (J. Bae).

0378-7753/$ – see front matter © 2010 Elsevier B.V. All rights reserved.
doi:10.1016/j.jpowsour.2010.09.018

Ni–YSZ hydrogen electrode/YSZ electrolyte/LSM–YSZ O_2 electrodes [10,17–20]. There are reports in the literature that the electrode area specific resistance (ASR) is higher in the electrolytic mode (SOEC) than in the galvanic mode (SOFC) [17,19]; however, there is also evidence that the ASRs of equivalent electrodes used in SOFCs and SOECs are identical [18]. These contrasting observations may be the result of the different operating conditions. Alternatives to the widely used Ni–YSZ and LSM–YSZ composite SOEC electrodes are also under investigation [21–23].

In addition to steam electrolysis, SOEC is capable of carbon dioxide electrolysis:

Carbon dioxide electrolysis:

$$CO_2 \rightarrow CO + 0.5O_2, \quad \Delta G = 189.2\,\text{kJ mol}^{-1} \tag{2}$$

Although the electrolysis of CO_2 thermodynamically demands more total energy than water, CO_2 electrolysis can be advantageous as it can help sequester CO_2 and/or reuse CO_2 from the energy system. The coelectrolysis of steam and CO_2 yields a synthesis gas ($CO + H_2$) that can be catalysed into various synthetic fuels [13]. For example, if the syngas production using SOEC coelectrolysis is followed by Fischer–Tropsch conversion, then it represents a means of recycling CO_2 into a useful liquid fuel. However, coelectrolysis is more complicated than steam electrolysis. It is not well understood whether H_2O and CO_2 are actually simultaneously electrolysed, or whether steam is electrolysed predominantly to produce H_2, which reacts with CO_2 to produce CO via the reverse water gas shift reaction (RWGS) [24]:

Reverse water gas shift reaction:

$$H_2 + CO_2 \rightarrow CO + H_2O, \quad \Delta G = 0.51\,\text{kJ mol}^{-1} \tag{3}$$

This study primarily focused on the material selection for SOEC electrode compartments. The electrode overpotentials for the positive (O_2 electrode) and negative electrodes (H_2 electrode) were determined under both anodic and cathodic polarisations. The performance discrepancies between SOFC and SOEC modes of each electrode were compared by examining the electrode overpotential across both regimes of operation. A ring-type Pt reference electrode and a circular Pt counter electrode were used to individually assess the overpotential for each electrode. We investigated the electrochemical performances of Ni–YSZ, Ni–$Gd_{0.1}Ce_{0.9}O_{1.95}$ (Ni–GDC), and Ni/Ruthenium–GDC (Ni/Ru–GDC) H_2 electrodes under various operating conditions (operating temperature, steam electrolysis, carbon dioxide electrolysis and coelectrolysis). We also investigated several composite O_2 electrodes: $La_{0.8}Sr_{0.2}MnO_{3-\delta}$–YSZ (LSM–YSZ), $La_{0.6}Sr_{0.4}Co_{0.8}Fe_{0.2}O_{3-\delta}$ (LSCF), and $La_{0.8}Sr_{0.2}FeO_{3-\delta}$ (LSF).

2. Experiments

2.1. Three-electrode cell preparation

SOEC electrolyte-supported cells with a reference electrode were prepared to evaluate the overpotential and durability of individual electrodes. A ring-type reference electrode was applied, consisting of platinum (Gwi-joo Metal, Korea). The three-electrode cell configuration (working electrode, counter electrode, and reference electrode) is presented in Fig. 1. The proper cell configuration is necessary to ensure uniform current distribution and to reduce errors that can occur when a reference electrode is introduced [25,26]. A reference electrode should be stable and placed in a stable gaseous environment; otherwise changes in the electrode and gas partial pressure can cause alterations in the reference potential. Our previous study showed that O_2 electrodes affected the discrepancies in the performance of the cell operated under SOFC and SOEC modes [27]. The Ni-containing H_2 electrode suffers from a coarsening of Ni particles at high steam-to-H_2 ratios

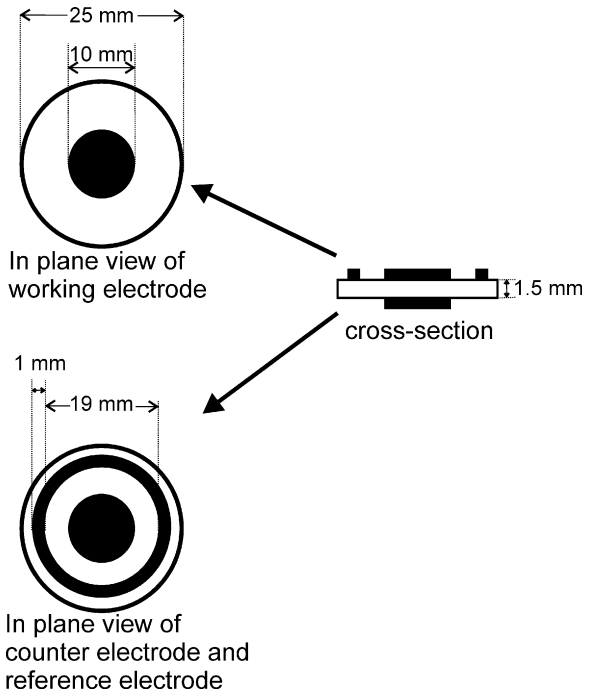

Fig. 1. Three-electrode/electrolyte-supported cell configuration.

[28]. Therefore, Pt was chosen as a reference and counter electrode in this study to maintain the electrode's performance stability in both modes of operation. YSZ powder (Tosho, Japan) was pressed at 1 metric ton for 30 s followed by sintering at 1500 °C for 4 h to produce pellets with a diameter of ~25.0 mm and a thickness of ~1.5 mm. The working electrode slurries were blended with compositions of 15 wt% of binder (Butvar B-98, Sigma–Aldrich), 1 wt% of dispersant (polyvinyl pyrrolidone, Sigma–Aldrich), 1 wt% of plasticiser (polyethylene glycol, Sigma–Aldrich), and electrode powder balance (Ni, J.T. Baker, USA; YSZ, Tosho, Japan; GDC, Praxiar, USA; Ru–GDC, Praxiar, USA; LSM, LSCF and LSF, HANCHANG, Korea). The working electrode and counter electrode were identical circular discs. The working electrodes were screen-printed on YSZ electrolyte and fired for 1 h (1200 °C for Ni–YSZ, Ni–GDC and Ni/Ru–GDC; 1100 °C for LSM–YSZ, LSCF and LSF), giving an electrode layer with an area of 0.785 cm^2 and a thickness of ~30 μm. A Pt counter electrode with an area of 0.785 cm^2, surrounded by a ring reference electrode (Pt), was screen-printed and fired at 900 °C for 1 h. The reference electrode had an internal diameter of 19 mm and external diameter of 21 mm. The weight ratio between LSM and YSZ in the composite electrode was 50:50. The weight ratio between Ni and YSZ in the composite electrode was 40:60. The weight ratio of Ni–GDC in the composite electrode was 40:60, and that of Ni:Ru:GDC was 40:0.5:59.5.

2.2. Electrochemical performance measurements

Single cell polarisation curves were generated using linear sweep current techniques. A potentiostat (Solartron, SI 1287) was used to control the voltage between 0.3 and 1.5 V with a scan rate of 20 mV s^{-1}. Electrochemical impedance spectroscopy (EIS) measurements were performed using a sinusoidal signal amplitude of 20 mV_{rms}, across the frequency range of 100 kHz to 0.1 Hz. The EIS was collected using a frequency response analyser (Solartron, SI 1260).

The electrical connection was made to the cell electrodes via platinum wires and paste (wire 99.99% Pt, 0.25 mm diameter, Gwi-joo Metal, South Korea) and was placed into compression. The cell

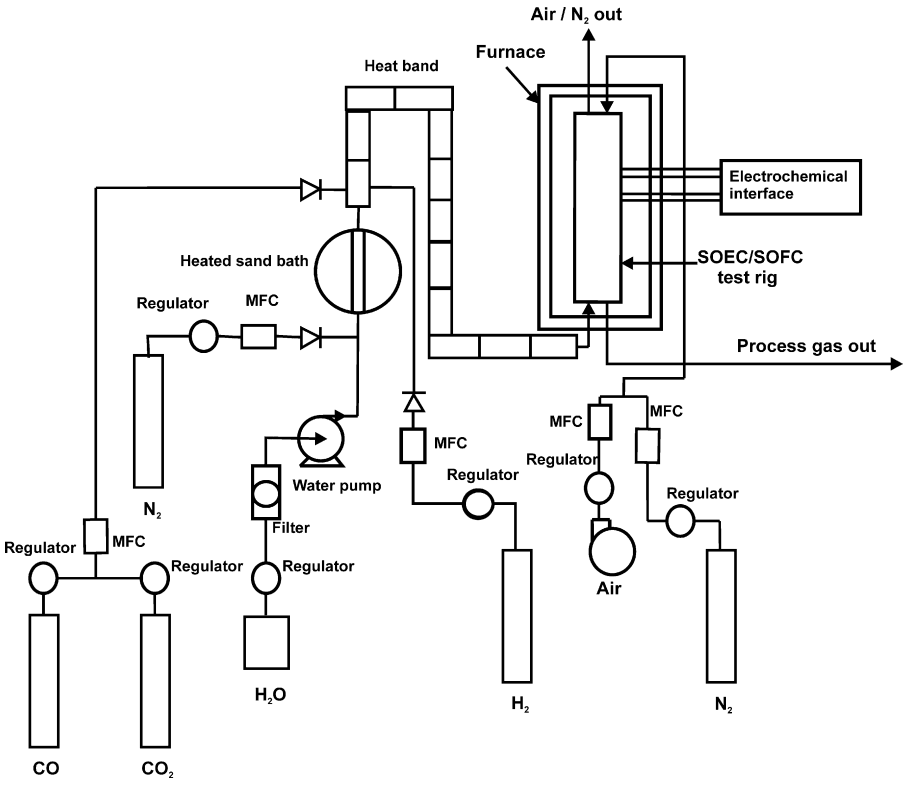

Fig. 2. Schematic drawing of the test system.

ridge was sealed using glass sealant (Untra-Temp 516, Aramco, USA) to separate the gas environment of the two electrodes. Fig. 2 shows the experimental set-up for the delivery of the gas to the cell in the furnace. The test system allowed variable gas compositions of steam, H_2, CO_2, CO, and N_2 to be introduced to the H_2 electrode, as well as air to the O_2 electrode. N_2 was used as a carrier gas to control the steam ratio in the gas compositions. Deionised water, supplied using an HPLC liquid pump (Chrom Tech, USA), was evaporated in a heated sand bath and mixed with the N_2 line. The steam/N_2 stream was combined with the H_2 and/or CO_2/CO and directed to the furnace using a heating line for steam, CO_2 or coelectrolysis.

3. Results

3.1. Performance degradation in SOECs

Fig. 3 shows that significant performance degradation was observed for a button cell (H_2 electrode support) when operated in steam electrolysis mode. The button cell (Ni–YSZ/YSZ/LSM–YSZ) degraded over 20% after 200 h. As shown in Fig. 3(a), after the SOEC mode, the cell operated in SOFC mode at a lower constant current density and different gas compositions relative to the H_2 electrode. The degraded performance from the SOEC operation was permanent degradation and was not recovered during the SOFC operations. The lower current density used in SOFC mode was mainly a response to the performance degradation from the previous SOEC mode. Fig. 3(b) shows the I/V response of the cell before and after 300 h of operation, which reflects a significant increase in the cell's ASR after the electrolysis mode. The cell had open circuit voltage (OCV) of 0.88 V for $H_2O/H_2 = 70/30$ before operation, closely agree with the Nernst potential (calculated from Gibbs free energy of formation, 0.90 V); however, the cell exhibited lower OCV (0.82 V) after 300 h of operation, which could indicate sealing leakage after prolong operation and could be an additional effect of cell's performance degradation. When compared to the cell exposed to dry H_2 ($H_2/N_2 = 50/50$), the use of steam ($H_2O/H_2 = 70/30$) produced more voltage noise but had no effect on the degradation trend (at constant current density of 0.01 A cm^{-2}). The source of the noise in the performance response is uncertain. There is the possibility of "flashing" during the water vaporisation process, resulting in uneven introduction of steam to the H_2 electrode and/or poor control of water addition in the experiment. Unlike in the SOEC mode, the cell was more stable in the SOFC mode for both gas compositions. The effect of lower current density (0.1 A cm^{-2} versus 0.01 A cm^{-2}) may have been the main reason for the variance in the performance stability. It was difficult to identify the cell discrepancies in the cell performance stability between two modes (SOFC versus SOEC) without further study; however, the results presented herein demonstrate the significant performance degradation of SOECs.

Discernable changes in the microstructure were observed in both the O_2 electrode and the H_2 electrode after SOEC operation. Delamination of the oxygen electrode layer from the electrolyte was observed for various electrodes after the cell was operated in the electrolysis modes. Our previous work [27] reported delamination in the O_2 electrode made of barium strontium cobalt ferrite (BSCF). The BSCF layer was partially delaminated after only 20 h of electrolysis, while the LSM–YSZ electrode remained fused to the electrolyte layer. Mawdsley et al. [29] reported that delamination of the LSM–YSZ oxygen electrode was a source of the performance degradation in the SOEC stack after a prolonged operation (2000 h). The cause of the delamination was not clear, but it was reported that a high rate of oxygen release into any defects at the perovskite–zirconia interfaces within the electrolyte layer could cause localised pressure-induced cracking at the interfaces [29].

Agglomeration of Ni particles and micro-cracks in the Ni–YSZ H_2 electrode were also observed in the previous work after 500 h of electrolysis using $H_2O/H_2 = 80/20$ with 50% steam utilisation [30]. These results stress that the electrode materials for the SOEC compartment should be further studied. The reference electrode

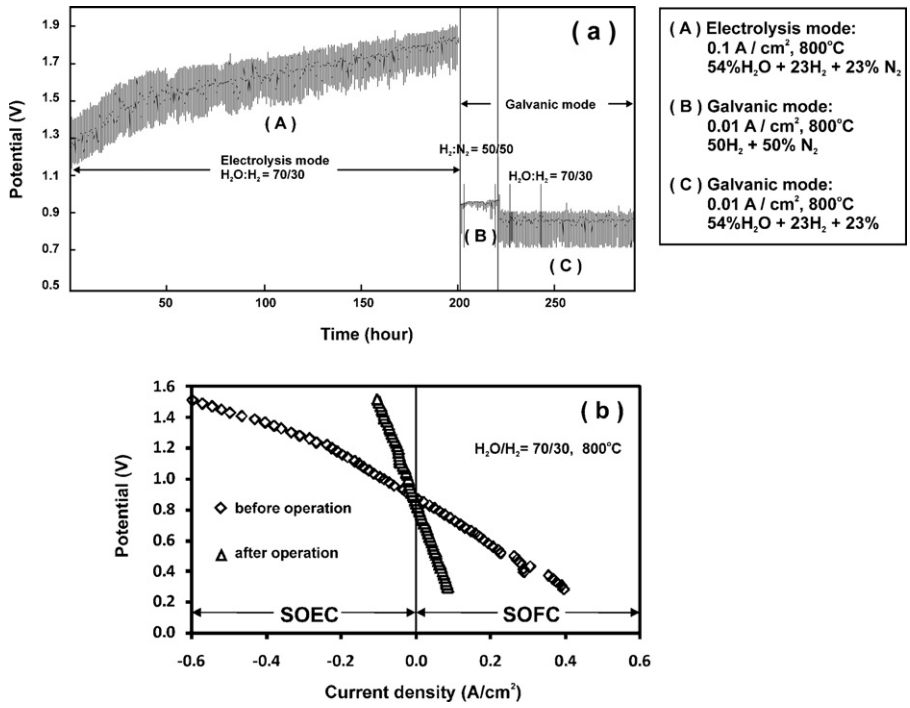

Fig. 3. (a) Durability test of the Ni–YSZ/YSZ/LSM–YSZ hydrogen electrode-supported button cell for the electrolysis mode and the galvanic mode (different current density and gas composition relative to H_2 electrode) at 800 °C, and (b) I/V response of the cell before and after the electrolysis/galvanic mode for 300 h. The cell had the OCV before operation of 0.88 V.

can be applied to individually assess the performance of each electrode.

3.2. Electrochemical performance of the H_2 electrode

3.2.1. Variation of temperature

The overpotential of the H_2-electrode was evaluated in both SOEC and SOFC modes. The operating temperatures were varied from 550 °C to 800 °C, whereas the steam content delivered to H_2-electrode was maintained constantly at H_2O/H_2 = 70/30 (54% H_2O + 23% H_2 + 23% N_2). To observe any discrepancies in the electrode performance between the SOEC and SOFC modes, Tafel plot was used to analyse the electrode overpotential. The overpotentials of the Ni–YSZ, Ni–GDC, and Ni/Ru–GDC electrodes are presented in Fig. 4(a–c), respectively. The overpotential decreased with increasing temperatures for all electrodes, as expected. Ni–YSZ showed asymmetric behaviour for steam electrolysis and H_2 oxidation. The activity of the Ni–YSZ electrode for H_2 oxidation was significantly higher than that for steam electrolysis. This agrees with the results reported by Eguchi et al. [17] and Marina et al. [22].

Various explanations have been proposed to account for the degradation of Ni electrodes when operating under SOEC conditions. It has been reported that higher polarisation losses for the H_2-electrode are predicted during electrolysis mode, mainly because of the difference in H_2 and H_2O diffusions [31]. It is also known that high steam content environments accelerate the agglomeration of Ni particles [32] and a change in the electrode microstructure as a result of Ni particle agglomeration leads to a decrease in the length of three phase boundaries (TPB) [22]. Thinner electrodes and smaller particles are reported to be more susceptible to rapid degradation at high steam partial pressure than the thick and coarse structure [22]. The surface oxidation of Ni under high steam containing environment, forming a less active layer, has been proposed as another possible cause of performance degradation of the electrode under electrolysis conditions [17]. It has been reported that the polarisation of the Ni electrode became large as the operating pO_2 approached that of the Ni–NiO system due to surface oxidation of metal [33], suggesting that the use of a precious metal may be preferable under high steam conditions [17].

In contrast to the Ni–YSZ electrode, comparable activity for operating between the SOEC and SOFC modes was achieved with the Ni–GDC and the Ni/Ru–GDC electrodes. Both electrodes showed higher electrochemical performance than the Ni–YSZ electrode over a range of temperatures (550–800 °C). All of the H_2 electrodes in this study contained the same amount of 40 wt% Ni (40 wt% Ni–60 wt% YSZ; 40 wt% Ni–60 wt% GDC; and, 40 wt% Ni/0.5 wt% Ru–59.5 wt% GDC). This result suggests that the GDC constituent in the electrodes favours operation in the electrolysis direction. It is likely that the oxygen storage capacity of GDC helps to suppress the oxidation of the Ni surface and leads to a higher performance in the electrolysis regime. The addition of 0.5 wt% Ru in the composite electrode largely increased the performance of the Ni–GDC electrode over the range of temperatures studied.

3.2.2. Variation of gas composition to the hydrogen electrode

Although GDC may be the preferred hydrogen electrode composition for SOECs, there is also a drawback to its use. The overpotential of the Ni–YSZ electrode during steam electrolysis (not shown) slightly decreased with increasing steam-to-hydrogen ratio (H_2O/H_2 ratio = 50/50 to 90/10), corresponding to the other work [22], whereas the overpotential for the Ni–GDC and the Ni/Ru–GDC electrodes slightly increased when H_2O/H_2 was changed from 50/50 to 70/30 and significantly increased when H_2O/H_2 = 90/10, shown in Fig. 5 for Ni/Ru–GDC electrode. This was likely a result of the sensitivity of the GDC conductivity to pO_2.

To investigate the SOEC performance during CO_2 electrolysis, the overpotential of the Ni–GDC electrode as a function of current density in the CO_2 electrolysis mode is shown in Fig. 6(a). The overpotential for CO_2 reduction increased with increasing CO_2/CO ratio from 50/50 to 70/30 and largely increased when the electrode was exposed to a CO_2/CO = 90/10 and 100/0 gas environment (operating temperature of 800 °C), corresponding to the increasing ASR shown

Table 1
Gas composition for each operating mode.

Operating mode	Gas composition		
H_2O electrolysis	H_2O/H_2 = 50/50, 38% H_2O + 38% H_2 + 24% N_2	H_2O/H_2 = 70/30, 54% H_2O + 23% H_2 + 23% N_2	H_2O/H_2 = 90/10, 69% H_2O + 8% H_2 + 23% N_2
Coelectrolysis H_2O/CO_2	22% CO_2 + 22% CO + 22% H_2O + 22% H_2 + 12% N_2		
CO_2 electrolysis	CO_2/CO = 50/50, 50% CO_2 + 50% CO	CO_2/CO = 70/30, 70% CO_2 + 30% CO	CO_2/CO = 90/10, 90% CO_2 + 10% C

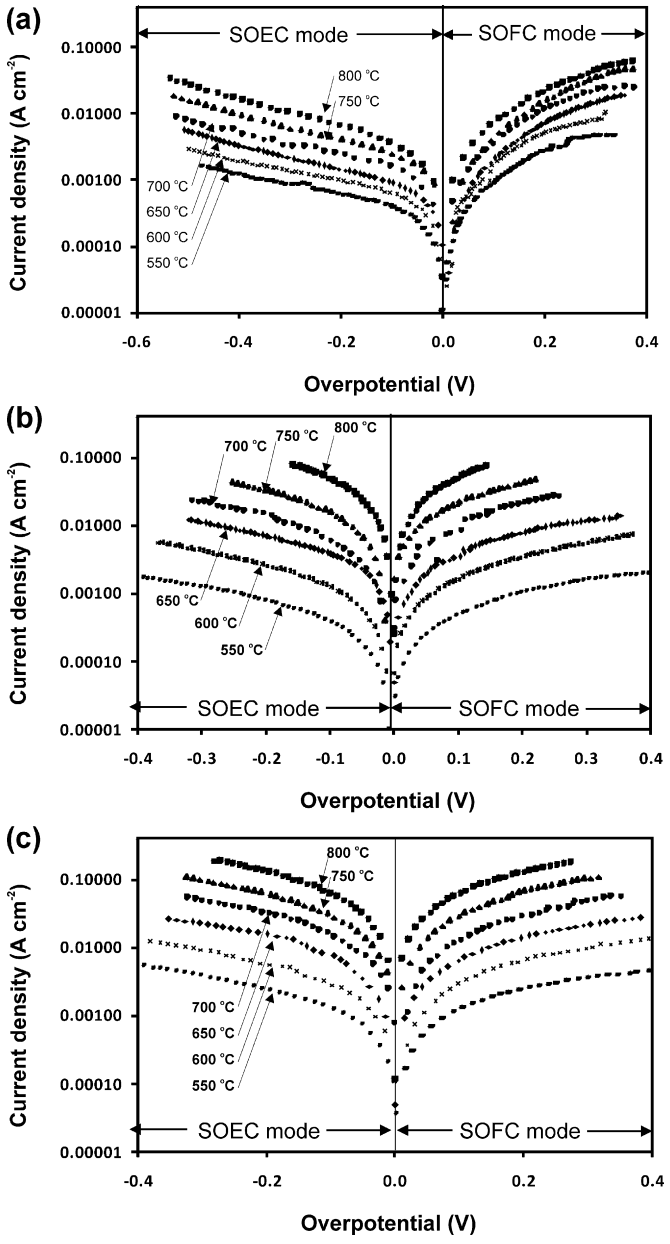

Fig. 4. Current/overpotential of: (a) Ni–YSZ, (b) Ni–GDC, and (c) Ni/Ru–GDC in the electrolysis and galvanic modes for temperatures ranging from 550 °C to 800 °C (H_2O/H_2 = 70/30 to H_2 electrode).

in Fig. 6(b). The exact gas composition for each operating mode is shown in Table 1.

Comparing the electrode (Ni–YSZ, Ni–GDC, Ni/Ru–GDC) when operated in varied operating conditions (H_2O electrolysis, CO_2 electrolysis, and coelectrolysis), it can be seen in Fig. 7 that all the electrodes exhibited comparable performance under steam electrolysis and coelectrolysis. The electrode performance was lower when operating in the CO_2-electrolysis mode. This suggests that the coelectrolysis of H_2O/CO_2 is preferred to CO_2-electrolysis. CO_2-

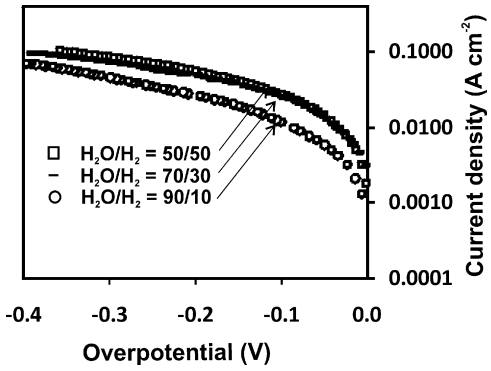

Fig. 5. Current/overpotential of the Ni/Ru–GDC H_2 electrode under steam electrolysis when H_2O/H_2 = 50/50, 70/30 and 90/10 at a constant operating temperature of 800 °C.

electrolysis actually requires a higher reduction potential than steam electrolysis. Moreover, when a high operating potential is applied, a high concentration of CO is formed via CO_2 electrolysis. High concentration CO can potentially be further reduced to element C via the Boudouard reaction ($CO \rightarrow C + 0.5O_2$) being shifted towards coke formation. At this condition, carbon deposition can occur. It was reported that CO with small amount of H_2 can induce carbon deposition on Ni–YSZ cermet and that the presence of a small amount of H_2 may assist the dissociation of adsorbed CO and, thus, promote carbon deposition [34].

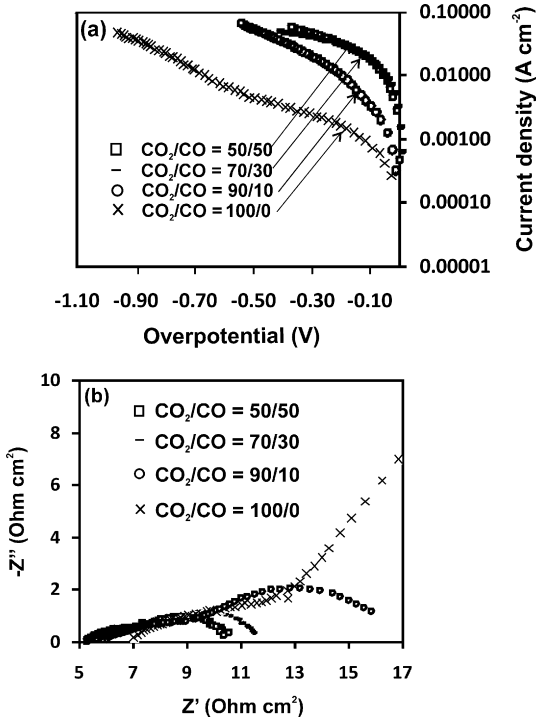

Fig. 6. (a) Current/overpotential and (b) electrochemical impedance response of the Ni–GDC electrode when exposed to different CO_2-to-CO ratios at a constant operating temperature of 800 °C.

Table 2
Operating conditions for durability test of Ni–YSZ electrode at 800 °C.

Operating mode		Current density (mA cm^{-2})	Gas composition (vol.%)
(a)	SOFC	10	54% H_2O + 23% H_2 + 23% N_2
(b)	SOEC: H_2O electrolysis	10	54% H_2O + 23% H_2 + 23% N_2
(c)	SOEC: CO_2 electrolysis	10	23% CO_2 + 23% CO + 15% H_2 + 39% N_2
(d)	SOFC	10	23% CO_2 + 23% CO + 15% H_2 + 39% N_2
(e)	SOEC: H_2O electrolysis	5	54% H_2O + 23% H_2 + 23% N_2
(f)	SOEC: co-H_2O/CO_2 electrolysis	5	23% CO_2 + 23% CO + 15% H_2 + 14% H_2O + 25% N_2

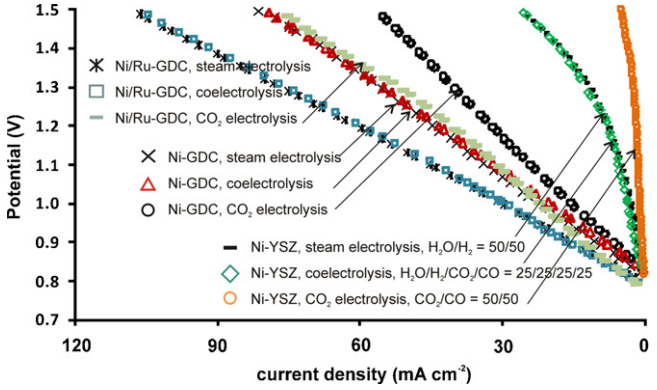

Fig. 7. Potential of electrolyte supported cells (H_2 electrode/YSZ electrolyte/Pt reference electrode), having Ni–YSZ, Ni–GDC and Ni/Ru–GDC H_2 electrode as a function of current density when the electrode operated under steam electrolysis (H_2O/H_2 = 50/50: 38% H_2O + 38% H_2 + 24% N_2), CO_2 electrolysis mode (CO_2/CO = 50/50: 25% CO_2 + 25% CO + 50% N_2), and coelectrolysis of H_2O/CO_2 (22% CO_2, 22% CO, 22% H_2O, 22% H_2, 12% N_2).

Although the ceria-based electrode was expected to suppress carbon deposition, in this study the ceria-based electrode exhibited a lower performance for CO_2-electrolysis than for coelectrolysis. Following the same trend during steam electrolysis as demonstrated by Ni–YSZ and Ni–GDC in this study, Ni/Ru–GDC provided the highest performance for coelectrolysis. It seems likely that the addition of 0.5 wt% Ru in the composite electrode increases the electrochemical performance of the Ni–GDC electrode in steam electrolysis, and the use of Ru in the composite electrode is also expected to favour the kinetics of the RWGS reaction (Eq. (3)), which is reported to occur during coelectrolysis of H_2O/CO_2.

3.3. Durability test of the H_2 electrode

Durability studies of the Ni–YSZ electrode in the electrolysis and fuel cell modes were performed at a constant operating temperature of 800 °C (100 h total operating time) under varied conditions (current density and gas composition for H_2O electrolysis, CO_2 electrolysis and coelectrolysis). The operating conditions for these experiments are listed in Table 2. As shown in Fig. 8, the electrode was initially exposed to H_2O/H_2 = 70/30 (54% H_2O + 23% H_2 + 23% N_2) at a constant current density in SOFC mode (Line (a)). Next, under the same gas composition (H_2O/H_2 = 70/30), the cell was taken into SOEC mode with the same current density and gas composition (Line (b)). The Ni–YSZ electrode exhibited stability for both fuel cell and steam electrolysis modes. In Line (c), the electrode performance was significantly degraded when CO_2 electrolysis was carried out at a constant current density (23% CO_2 + 23% CO + 15% H_2 + 39% N_2). The cell performance also rapidly decreased under the same gas conditions in fuel cell mode (Line (d)). The degraded performance was only partially recovered using the steam electrolysis mode (Line (e)). Finally, the electrode was more stable when exposed to the coelectrolysis condition (Line (f)). Steam contained in the coelectrolysis gas composition may help to suppress the occurrence of carbon deposition and lead to more stability in electrode performance in coelectrolysis mode when compared to the CO_2 electrolysis mode. The post mortem SEM analysis should be thorough examined. A further, more complete, study of post-operation analysis in electrolysers will be formed.

3.4. Electrochemical performance of the O_2 electrode

3.4.1. Variation of temperature

The overpotential of the O_2 electrode was evaluated under both SOEC and SOFC operating modes. The operating temperatures were varied from 700 °C to 800 °C, while the airflow rate to the O_2 electrode was kept constant at 100 ml min^{-1}. The order of performance for the O_2 electrodes was LSCF > LSF > LSM–YSZ in the SOEC and the SOFC modes. The overpotentials for LSM–YSZ, LSCF, and LSF are shown in Fig. 9(a–c), respectively, and the overpotential decreased with increases in the temperature for all of the samples. All of the electrodes exhibited asymmetrical behaviour between the anodic and cathodic conditions. The activity of all the O_2 electrodes as an SOFC cathode is higher than that as SOEC anodes. Among the O_2 electrodes, LSM–YSZ exhibited the nearest to symmetrical behaviour, consistent with earlier work [22] to which the electrochemical performances of LSM, LSCuF, and LSCoF were compared. It has been reported that the asymmetrical behaviour is most apparent for the mixed-conducting LSCuF and LSCoF electrodes, while it is discernable for LSM. Marina et al. [22] have discussed the depletion of oxygen vacancies in mixed ionic/electronic conductivity (MIEC) electrodes under the SOEC anodic conditions – corresponding to the modelling work of Svensson et al. [35]. The

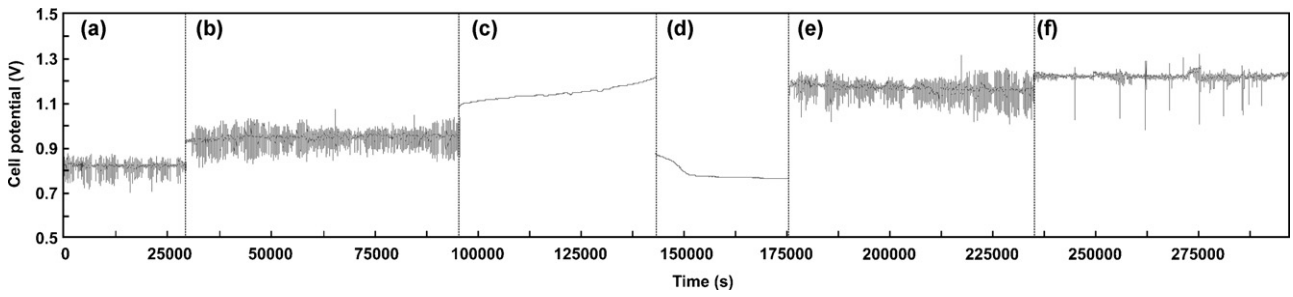

Fig. 8. Durability test of Ni–YSZ electrode under varied conditions (gas compositions, current density 5–10 mA cm^{-2}, 800 °C): (a) SOFC mode, (b) H_2O electrolysis, (c) CO_2-electrolysis, (d) SOFC mode, (e) H_2O electrolysis, and (f) co-H_2O/CO_2 electrolysis. The cell had the OCV before operation of 0.88 V.

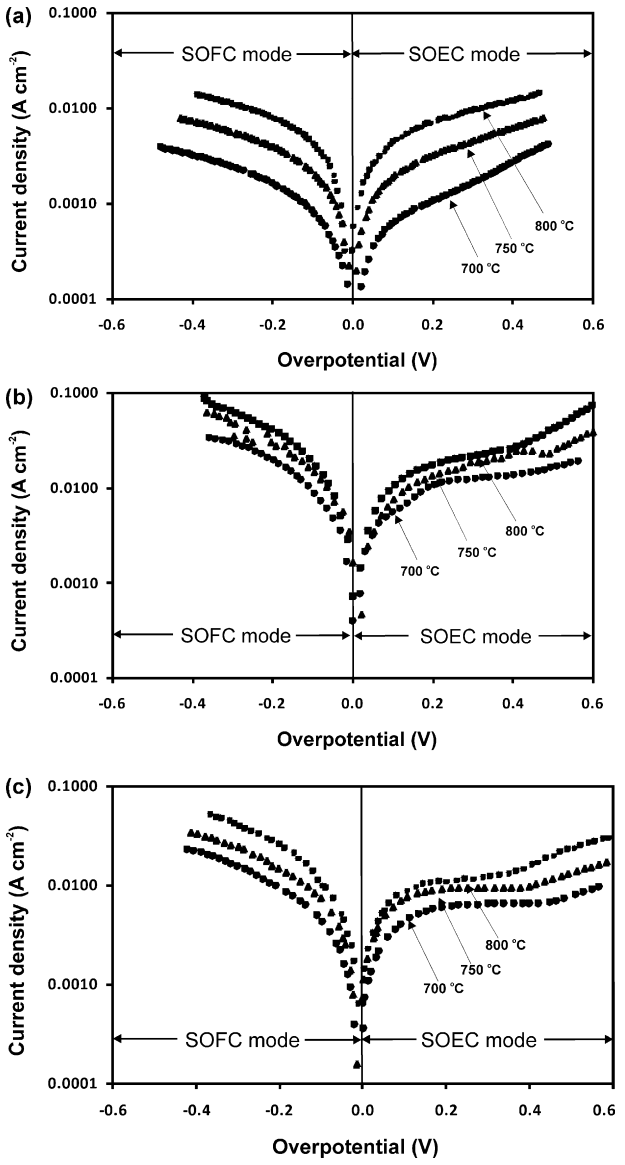

Fig. 9. Current/overpotential of: (a) LSM–YSZ, (b) LSCF, and (c) LSF under the electrolysis and galvanic modes for a range of temperatures from 700 °C to 800 °C (ambient air to O_2 electrode).

high local partial pressure of oxygen produced at the TPB operation can affect the performance stability of the oxygen electrode, which is optimised for stability under the cathodic (fuel cell) but not anodic (electrolyser) operating conditions. This suggests that an oxygen electrode that is able to accommodate a large oxygen overstoichiometry under oxidising conditions may be required for SOEC operation.

4. Conclusion

Electrochemical performance of both H_2 electrodes and O_2 electrodes were investigated during steam electrolysis, CO_2 electrolysis, and coelectrolysis of H_2O/CO_2 using varied gas composition and operating temperature. The overpotential decreased with increasing temperature for all of the electrodes. The electrochemical performance of the Ni–YSZ electrode for H_2 oxidation was significantly higher than that for steam electrolysis. Comparable activity for operating between the SOEC and SOFC modes was achieved with the Ni–GDC and the Ni/Ru–GDC electrodes. Both electrodes also showed higher electrochemical performance than the Ni–YSZ electrode over a range of temperatures (550–800 °C). The result suggests that the GDC constituent in the electrodes favours operation in the electrolysis direction. However, there is also a drawback to the use of GDC since the overpotential for the GDC containing electrodes increased when increasing H_2O/H_2 ratio from 50/50 to 90/10. All of the O_2 electrodes exhibited asymmetrical behaviour for anodic and cathodic conditions.

The overpotential for CO_2 reduction increased with increasing CO_2/CO ratio, corresponding to the increasing ASR. All the H_2 electrodes in this study exhibited comparable performance under steam electrolysis and coelectrolysis while the performance was lower when operating in the CO_2-electrolysis mode. This suggests that the coelectrolysis of H_2O/CO_2 is preferred to CO_2-electrolysis. Following the same trend during steam electrolysis this study, Ni/Ru–GDC provided the highest performance for coelectrolysis.

The activity of all the O_2 electrodes as an SOFC cathode in this study was higher than that as an SOEC anode. The LSM–YSZ exhibited the nearest to symmetrical behaviour among the O_2 electrodes in this study. The order of performance for the O_2 electrodes was LSCF > LSF > LSM–YSZ in both SOEC and SOFC modes.

Acknowledgements

This work is funded by the Korea Electric Power Research Institute (KEPRI), Republic of Korea.

The work is also the outcome of "the Development Programme for Core Technologies for Fuel Cells (CTFC)" and "Solid Oxide Fuel Cell of New and Renewable Energy Research and Development Programme (20093021030010)" of the Ministry of Knowledge Economy (MKE). Furthermore, this work was supported by "the Brain Korea 21 (BK21) Programme" and "The Encouragement Programme for the EU FP Participation" funded by the Ministry of Education, Science Technology (MEST), Republic of Korea.

References

[1] M. Ball, M. Wietschel, Int. J. Hydrogen Energy 34 (2009) 615–627.
[2] N. Laosiripojana, S. Assabumrungrat, Appl. Catal. B 82 (2008) 103–113.
[3] N. Laosiripojana, S. Assabumrungrat, J. Power Sources 158 (2006) 1348–1357.
[4] S.-H. Yoon, I.-Y. Kang, J.-M. Bae, Int. J. Hydrogen Energy 34 (2009) 1844–1851.
[5] S.-H. Yoon, J.-M. Bae, S.-Y. Kim, Y.-S. Yoo, J. Power Sources 192 (2009) 360–366.
[6] J. Pettersson, B. Ramsey, D. Harrison, J. Power Sources 157 (2006) 28–34.
[7] W. Smith, J. Power Sources 86 (2000) 74–83.
[8] T. Ioroi, K. Yasuda, Z. Siroma, N. Fujiwara, Y. Miyazaki, J. Power Sources 112 (2002) 583–587.
[9] M. Ferraro, F. Sergi, G. Brunaccini, G. Dispenza, L. Andaloro, V. Antonucci, J. Power Sources 193 (2009) 342–348.
[10] S.H. Jensen, P.H. Larsen, M. Mogensen, Int. J. Hydrogen Energy 32 (2007) 3253–3257.
[11] M.A. Laguna-Bercero, S.J. Skinner, J.A. Kilner, J. Power Sources 192 (2009) 126–131.
[12] N.Q. Minh, T. Takahashi, Science and Technology of Ceramic Fuel Cells, Elsevier, Amsterdam, Netherland, 1995.
[13] S.D. Ebbesen, M. Mogensen, J. Power Sources 193 (2009) 349–358.
[14] J. Udagawa, P. Aguiar, N.P. Brandon, J. Power Sources 180 (2008) 354–364.
[15] W. Dönitz, G. Dietrich, E. Erdle, R. Streicher, Int. J. Hydrogen Energy 13 (1988) 283–287.
[16] B. Yidiz, M.S. Kazimi, Int. J. Hydrogen Energy 31 (2006) 77–92.
[17] K. Eguchi, T. Hatagishi, H. Arai, Solid State Ionics 86–88 (1996) 1245–1249.
[18] J.E. O'Brien, C.M. Stoots, J.S. Herring, P.A. Lessing, J.J. Hartvigsen, S. Elangovan, J. Fuel Cell Sci. Technol. 3 (2005) 156–163.
[19] A. Hauch, S.H. Jensen, S. Ramousse, M. Mogensen, J. Electrochem. Soc. 153 (2006) A1741–A1747.
[20] A. Brisse, J. Schefold, M. Zahid, Int. J. Hydrogen Energy 33 (2008) 5375–5382.
[21] W. Wang, Y. Huang, S. Jung, J.M. Vohs, R.J. Gorte, J. Electrochem. Soc. 153 (2006) A2066–A2070.
[22] O.A. Marina, L.R. Pederson, M.C. Williams, G.W. Coffey, K.D. Meinhardt, C.D. Nguyen, E.C. Thomsen, J. Electrochem. Soc. 154 (2007) B452–B459.
[23] F. Chauveau, J. Mougin, J.M. Bassat, F. Mauvy, J.C. Grenier, J. Power Source 195 (2010) 744–749.
[24] C. Stoots, J. O'Brien, J. Hartvigsen, Int. J. Hydrogen Energy 34 (2009) 4208–4215.
[25] M. Mogensen, P.V. Hendriksen, in: S.C. Singhal, M. Dokiya (Eds.), The Electrochemical Society Proceeding, 2003, p. 1126, PV 2003-7.
[26] G.J. Offer, P. Shearing, J.I. Golbert, D.J.L. Brett, A. Atkinson, N.P. Brandon, Electrochem. Acta 53 (2008) 7614–7621.

[27] P. Kim-Lohsoontorn, D.J.L. Brett, N. Laosiripojana, Y.-M. Kim, J.-M. Bae, Int. J. Hydrogen Energy 35 (2010) 3958–3966.
[28] A. Hauch, S.D. Ebbesen, S.H. Jensen, M. Mogensen, J. Electrochem. Soc. 155 (2008) B1184–B1193.
[29] J.R. Mawdsley, J.D. Carter, A.J. Kropf, B. Yildiz, V.A. Maroni, Int. J. Hydrogen Energy 34 (2009) 4198–4207.
[30] H.-B. Yim, S.-G. Yu, K.-J. Park, P. Kim-Lohsoontorn, J.-M. Bae, Performance of 5 cm × 5 cm Solid Oxide Electrolysis Cell, NECS Lab, KAIST, Subcontract Report to KAPRI, 2009.
[31] J. Guan, N. Minh, B. Ramamurthi, J. Ruud, J.-K. Hong, P. Riley, D. Weng, High performance flexible reversible solid oxide fuel cell. GE Global Research Center Final Report for DOE Cooperative Agreement DE-FC36-04GO-14351. 2006.
[32] J. Sehested, Catal. Today 111 (2006) 103–110.
[33] K. Eguchi, Y. Kunisa, K. Adachi, M. Kayano, K. Skizawad, H. Arai, Chem. Lett. 24 (1995) 963–964.
[34] V. Alzate-Restrepo, J.M. Hill, J. Power Sources 195 (2009) 1344–1351.
[35] A.M. Svensson, S. Sunde, K. Nisancioglu, J. Electrochem. Soc. 145 (1998) 1390–1399.